

Received 27 January 2024; revised 25 March 2024; accepted 26 March 2024.

Digital Object Identifier 10.1109/JMW.2024.3385047

Modeling Transmission Lines With Open Boundaries via Infinite Mapping Layer

GINES GARCIA-CONTRERAS¹, **JUAN CÓRCOLES**² (Senior Member, IEEE), **JORGE A. RUIZ-CRUZ**²,
MATTEO OLDONI³ (Member, IEEE), **LORENZO CODECASA**³ (Member, IEEE),
AND GIAN GUIDO GENTILI³

(Regular Paper)

¹Departamento de Tecnología electrónica y de las Comunicaciones, Escuela Politécnica Superior, Universidad Autónoma de Madrid, 28049 Madrid, Spain

²Information Processing and Telecommunications Center, Universidad Politécnica de Madrid, 28040 Madrid, Spain

³Dipartimento di Elettronica, Informazione e Bioingegneria, Politecnico di Milano, 20133 Milan, Italy

CORRESPONDING AUTHOR: Gines Garcia-Contreras (e-mail: gines.garcia@uam.es).

The work of Gines Garcia-Contreras, Juan Córcoles and Jorge A. Ruiz-Cruz was supported in part by the Spanish Government under Grant PID2020-116968RB-C32 (DEWICOM) and Grant TED2021-130650B-C21 (ANT4CLIM) funded by MCIN/AEI/10.13039/501100011033 (Agencia Estatal de Investigación) and in part by EU (European Union) "NextGenerationEU"/PRTR. The work of Matteo Oldoni, Lorenzo Codecasa, and Gian Guido Gentili was supported by the European Union under the Italian National Recovery and Resilience Plan (PNRR) of NextGeneration EU, partnership on "Telecommunications of the Future" (PE00000001 - Program "RESTART", Structural Project SRE).

ABSTRACT In this paper we introduce the use of several different Infinite Mapping Layers to model open boundaries in the 2-D Finite Element Method for the computation of transmission line parameters. The transformation maps a semi-infinite interval to a finite interval, thereby providing a simple and accurate description of open boundaries while keeping the size of the computational domain very compact. The method has been evaluated and tested on a variety of common transmission line geometries appearing in the literature and its accuracy is validated by comparing the results with canonical cases having closed expressions and with arbitrary geometries computed with commercial software tools. Various geometrical transformations have been developed and tested, and their performances evaluated in terms of accuracy and efficiency. Finally, the possibility of using a radial Infinite Mapping Layer has also been considered.

INDEX TERMS Electrostatics, finite element method (FEM), geometric transformation, open boundaries, transformation optics, transmission lines.

I. INTRODUCTION

Electrostatics is a field of great interest in computational applied physics due to its appearance in many practical problems [1]. In microwave engineering, electrostatic analysis is mainly devoted to the characterization of transmission lines [2], [3], [4], some of which have open boundaries (i.e. their fields are not entirely confined within conductors). Problems in which open boundaries are present are often found in both power systems [5] and conventional communication systems [6], [7], in which transmission line parameter computation is a typical post-processing analysis.

Open boundaries in electrostatics represent a challenge from an analysis standpoint. In classical texts, Conformal Mapping in general [2], and the Schwarz-Christoffel transformation in particular, were first identified as suitable tools

for the analysis of transmission lines with open boundaries, obtaining very satisfactory results for arbitrary geometries containing infinitely thin conductors [8].

When considering open transmission line characterization through the Finite Element Method (FEM) [9], [10], in order to make the problem solvable, a technique to truncate the computational domain is required. In this case, the usefulness of the Schwarz-Christoffel transformation becomes limited, since special care must be put in the meshing process to ensure that the discretization in the transformed domain does not lead to significant numerical errors [11]. Thus, other specific solutions to treat the open boundary problem in electrostatics were developed, such as the infinite elements [12], [13], the multipole expansion [14], and the well-known FEM-BEM (Boundary Element Method) technique [15]. Each of them has

its pros and cons, and very often the choice of the technique depends strongly on the problem under study. In the case of electrodynamics, other commonly used tools to mathematically approximate open boundaries in FEM are the Absorbing Boundary Conditions (ABC) [16], and Perfectly Matched Layers (PML) [17].

In this work we will model open-bounded electrostatic problems with Infinite Mapping Layers (IML) [18], [19], which are based on a coordinate transformation originally proposed in [20] with an inverse tangent expression to better describe evanescent fields in the frame of mode computation with Maxwell's equations. The coordinate transformation, which shares some similarities with transformation optics [21], [22], [23], has the purpose of mapping an infinite extent to a finite domain through an anisotropic electrical permittivity that sets the equivalence between the original problem in the original reference frame and the transformed one after the mapping. This approach can be an interesting alternative for electrostatics, and is introduced here for 2-D transmission line problems, although it can be easily extended to 3-D problems.

In [19], IML were initially explored in the context of mechanics, electrostatics, and deep wave propagation, with test examples based on structured meshes. For this work, in order to quantify the advantage of the proposed approach for transmission lines, several geometries and transformations have been developed and analyzed. Some observed advantages of the discussed formulation over other techniques include its straightforward FEM implementation, simplicity, and excellent performance, as demonstrated later. This is due to the method not necessitating any alterations to the FEM formulation, shape functions, and mesh elements.

Contrary to what is commonly found in the literature, meshes in IML do not need to be structured. The convergence of the line parameters is shown to greatly improve as compared to simple domain truncation, and the computational domain can always be kept very compact, leading to a greater reliability of the results and a significant reduction in computational time. Importantly, it has also been found that IML require a certain mesh density, although they can be placed very close to the problem geometry. Finally, a new type of radial IML has also been implemented and tested.

The organization of the paper is the following: we first briefly recall the formulation of the electrostatic problem related to transmission line parameter computation, and then we introduce FEM discretization together with the coordinate transformation. Finally, we discuss the results obtained, with several comparisons with available data and a study of convergence.

II. THE ELECTROSTATIC PROBLEM

A. MATHEMATICAL DEFINITION

Transmission line parameters can be obtained by solving the 2-D Laplace equation for the potential with Dirichlet-type boundary conditions in a system with perfect conductors ($\sigma =$

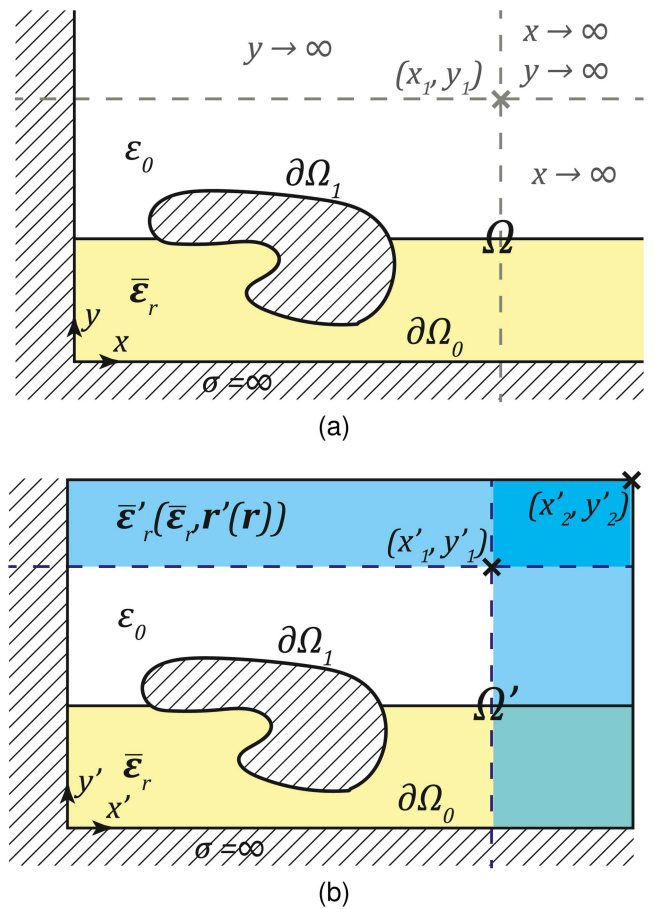


FIGURE 1. Problem under analysis. (a) Electrostatic problem in which the open boundaries are assumed to be from $x = x_1$ to infinity, and to $y = y_1$ to infinity. (b) Equivalent problem, in which the open boundaries have been modeled as an artificial material dependent on a geometrical transformation.

∞). Letting $\Phi = \Phi(x, y)$ be the potential function, we can define the problem as

$$\nabla \cdot (\bar{\epsilon}_r \nabla \Phi) = 0, \quad \text{in } \Omega \quad (1)$$

with the following boundary conditions

$$\begin{cases} \Phi = 1, & \text{on } \partial\Omega_1 \\ \Phi = 0, & \text{on } \partial\Omega_0 \end{cases} \quad (2)$$

$\partial\Omega_1$ being the boundary on which we apply unit voltage, $\partial\Omega_0$ the ground boundary (zero voltage), and $\bar{\epsilon}_r = \bar{\epsilon}_r(x, y)$ the relative electric permittivity double tensor [see Fig. 1(a)]. The Laplace equation is applicable both in case of homogeneous materials, for which rigorous Transverse Electromagnetic (TEM) propagation takes place [2], and in case of non-homogeneous materials (for instance piecewise homogeneous) for which the so called quasi-TEM propagation regime is a valid approximation up to some GHz [24], [25].

The solution of (1) allows to compute the capacitance C per unit length (p.u.l.) as

$$C = \epsilon_0 \int_{\Omega} \nabla \Phi \cdot \bar{\epsilon}_r \nabla \Phi \, d\Omega. \quad (3)$$

The inductance L p.u.l. can be obtained by $L = \mu_0 \epsilon_0 / C_0$, with μ_0 being the absolute permeability of vacuum, ϵ_0 the absolute permittivity of vacuum and C_0 the capacitance p.u.l. when the material is replaced by vacuum. The characteristic impedance Z_c is obtained as

$$Z_c = \sqrt{\frac{\mu_0 \epsilon_0}{C C_0}}. \quad (4)$$

Finally, the effective relative permittivity $\epsilon_{r,\text{eff}}$ and the propagation phase constant β can be obtained through

$$\epsilon_{r,\text{eff}} = \frac{C}{C_0} \quad \beta = \omega \sqrt{\mu_0 \epsilon_0 \epsilon_{r,\text{eff}}} \quad (5)$$

where ω is the angular frequency. Note that Z_c and β fully characterize a transmission line in the lossless case [2].

This procedure can also be performed if the problem exhibits more than two independent conductors (with different potential functions). In this case, one can define a capacitance matrix, whose coefficients are computed by a very similar technique [26].

B. SOLVING THE PROBLEM USING FEM

One of the most popular ways to solve Laplace equation is the Finite Element Method (FEM). We define the solution to (1) and (2) in a weak sense, by looking for Φ such that

$$\begin{aligned} \int_{\Omega} \nabla \Phi \cdot \bar{\epsilon}_r \nabla \Phi \, d\Omega &= 0 \\ \Phi &= 1, \quad \text{on } \partial\Omega_1 \\ \Phi &= 0, \quad \text{on } \partial\Omega_0 \end{aligned} \quad (6)$$

for each Φ belonging to $H^1(\Omega)$, the space of functions that are square integrable in Ω together with their gradient. The potential function Φ is then approximated as

$$\Phi(\mathbf{r}) = \sum_{i=1}^N v_i \varphi_i(\mathbf{r}) + \sum_{m=1}^M \bar{\varphi}_m(\mathbf{r}) \quad (7)$$

where the φ_i 's are standard FEM basis functions of interpolatory type on subdomains (typically triangles), the v_i 's are unknown coefficients and the $\bar{\varphi}_m$'s are analogous interpolatory functions in Ω whose sum is 1 at each point on $\partial\Omega_1$. Functions $\bar{\varphi}_m$ are thus used to impose the essential boundary condition on $\partial\Omega_1$. The essential boundary condition on $\partial\Omega_0$ is imposed simply by avoiding to include in the sum (7) the functions φ_n with non-zero trace on $\partial\Omega_0$. Equation (6) is then tested with the same set of basis functions $\{\varphi_i\}$ to find the matrix equation

$$\mathbf{K} \mathbf{v} = \mathbf{u} \quad (8)$$

where

$$\mathbf{v} = [v_1 \ v_2 \ \dots \ v_N]^T \quad \mathbf{u} = [u_1 \ u_2 \ \dots \ u_N]^T. \quad (9)$$

The generic element K_{ij} of the $[N \times N]$ matrix \mathbf{K} is

$$K_{ij} = \int_{\Omega} \nabla \varphi_i \cdot \bar{\epsilon}_r \nabla \varphi_j \, d\Omega. \quad (10)$$

We have then that the generic element u_i of the known term is given by

$$u_i = - \sum_{m=1}^M \int_{\Omega} \nabla \varphi_i \cdot \bar{\epsilon}_r \nabla \bar{\varphi}_m \, d\Omega. \quad (11)$$

After solving (8) and obtaining $\mathbf{v} = \mathbf{K}^{-1} \mathbf{u}$, the capacitance per unit length is then found from (3) as

$$C = \epsilon_0 (\mathbf{v}^T \mathbf{K} \mathbf{v} - 2 \mathbf{v}^T \mathbf{u} + w) = \epsilon_0 (w - \mathbf{v}^T \mathbf{u}) \quad (12)$$

where

$$w = \sum_{m=1}^M \sum_{n=1}^M \int_{\Omega} \nabla \bar{\varphi}_m \cdot \bar{\epsilon}_r \nabla \bar{\varphi}_n \, d\Omega. \quad (13)$$

III. MODELING OPEN BOUNDARIES AS AN ANISOTROPIC MATERIAL

To illustrate how the geometrical transformation is performed, we will use x, y as the coordinates of the original domain with infinite region, sketched in Fig. 1(a). Variable x, y , or both, extend to infinity according to the subregion they belong to. Referring to Fig. 1(a) and for simplicity to x coordinate only, the transformation used maps the semi-infinite domain $x_1 \leq x < \infty$ to the finite domain $x'_1 \leq x' < x'_2$ (where $x'_1 = x_1$) [see Fig. 1(b)].

According to the type of region, one can transform either variable or both using a generic coordinate transformation $(x, y) \rightarrow (x', y')$, depending on the semi-infinite domain involved in the solution process. The transformation should ensure continuity of the function and the first derivative, to get a smooth transition from untransformed to transformed domain.

As an effect of the geometrical transformation, an equivalent electrostatic problem can be defined by introducing an anisotropic inhomogeneous permittivity derived from the Jacobian matrix of the transformation itself [23]. Using $\bar{\epsilon}_r$ to indicate permittivity in the original domain and $\bar{\epsilon}'_r$ to indicate the new artificial material originating from the transformation, one gets the following, where $\bar{\mathbf{J}}$ is the Jacobian matrix of the transformation:

$$\bar{\epsilon}'_r = \frac{\bar{\mathbf{J}} \bar{\epsilon}_r \bar{\mathbf{J}}^T}{\det(\bar{\mathbf{J}})} \quad \bar{\mathbf{J}} = \begin{bmatrix} \bar{J}_{xx} & \bar{J}_{xy} \\ \bar{J}_{yx} & \bar{J}_{yy} \end{bmatrix} = \begin{bmatrix} \frac{\partial x'}{\partial x} & \frac{\partial y'}{\partial x} \\ \frac{\partial x'}{\partial y} & \frac{\partial y'}{\partial y} \end{bmatrix}. \quad (14)$$

Note that, if a formulation were to be developed for problems with inhomogeneous magnetic permeability, an equivalent expression to (14) for $\bar{\boldsymbol{\mu}}_r$ could be easily found [20]. It should be kept in mind that either x or y or both can undergo the transformation, so that the expression of the Jacobian matrix depends on the specific region in Fig. 1. For instance, if only x is transformed we will have $\partial y' / \partial y = 1$.

The new equivalent artificial material represented by (14) is inserted into (10), (11), and the solution obtained is theoretically equivalent to that of the original problem in an infinite domain. Moreover, letting Φ' be the solution in the transformed domain Ω' and Φ the solution in the original

domain Ω we have

$$\int_{\Omega} \nabla \Phi \cdot \bar{\epsilon}_r \nabla \Phi \, d\Omega = \int_{\Omega'} \nabla' \Phi' \cdot \bar{\epsilon}'_r \nabla' \Phi' \, d\Omega' \quad (15)$$

for which a proof is given in the Appendix.

Equation (15) ensures that the capacitance p.u.l. obtained by solving the transformed equation is equal to the capacitance in the original infinite domain.

IV. SOME POSSIBLE TRANSFORMATIONS FOR IML

The method here discussed does not impose any restrictions on the shape of the transformation nor in the discretization of the stretched region. However, monotonously decreasing functions for which it is possible to obtain (14) are found to be most suitable. For the problem of transmission lines we have considered three interesting coordinate transformations, here defined for a generic axis u , which map the range (u_1, ∞) to (u'_1, u'_2) , with $u_1 = u'_1$ (i.e., for $u' \geq u'_1$). They are:

$$u'_A = \frac{2}{\pi} (u'_2 - u'_1) \arctan \left(\frac{u - u_1}{u'_2 - u'_1} \frac{\pi}{2} \right) + u'_1 \quad (16)$$

$$u'_B = u'_2 - (u'_2 - u'_1) \exp \left(-\frac{u - u_1}{u'_2 - u'_1} \right) \quad (17)$$

$$u'_C = \frac{u'_2 u - u_1^2}{u + u'_2 - 2u_1}. \quad (18)$$

For these coordinate transformations we can obtain compact expressions for their derivatives (for $u' \geq u'_1$):

$$\frac{\partial u'_A}{\partial u} = \cos^2 \left(\frac{u' - u_1}{u'_2 - u_1} \frac{\pi}{2} \right) \quad (19)$$

$$\frac{\partial u'_B}{\partial u} = \frac{u'_2 - u'}{u'_2 - u_1} \quad (20)$$

$$\frac{\partial u'_C}{\partial u} = \left(\frac{u'_2 - u'}{u'_2 - u_1} \right)^2. \quad (21)$$

In Cartesian coordinates, $u = \{x, y\}$. With these expressions the the Jacobian matrix can be directly obtained. For example, taking (16) and for the upper-right region ($x' \geq x'_1$ and $y' \geq y'_1$) in Fig. 1(a) we would have:

$$\bar{\mathbf{J}} = \begin{bmatrix} \cos^2 \left(\frac{x' - x_1}{x'_2 - x_1} \frac{\pi}{2} \right) & 0 \\ 0 & \cos^2 \left(\frac{y' - y_1}{y'_2 - y_1} \frac{\pi}{2} \right) \end{bmatrix}. \quad (22)$$

Similar expressions can be obtained for the other presented transformations. If the transformation domain is symmetric (i.e. both $-\infty < x \leq -x_1$ and $x_1 \leq x < \infty$, $-\infty < y \leq -y_1$ and $y_1 \leq y < \infty$ are transformed), then the Jacobian can conveniently be expressed as, in this case for the transformation in (18):

$$\bar{\mathbf{J}}_{xx} = \begin{cases} \left(\frac{x'_2 - x'}{x'_2 - x_1} \right)^2, & \text{for } |x'| \geq x'_1 \\ 1, & \text{otherwise} \end{cases}$$

$$\bar{J}_{yy} = \begin{cases} \left(\frac{y'_2 - y'}{y'_2 - y_1} \right)^2, & \text{for } |y'| \geq y'_1 \\ 1, & \text{otherwise} \end{cases} \quad (23)$$

$$\bar{J}_{xy} = \bar{J}_{yx} = 0.$$

The procedure here described can easily be replicated with the transformations in (16) and (17).

For a radial transformation in (ρ, ϕ) , we again start from the expressions in (16)–(18) and take $u = \rho$. The geometrical transformation is now defined as $(\rho, \phi) \rightarrow (\rho', \phi')$, in which $\phi = \phi'$. Since the Laplace equation is being solved with FEM through a Cartesian coordinate system, it is additionally needed to derive the Jacobian of the desired radial transformation in Cartesian coordinates before solving the problem.

V. RESULTS

To check the validity and effectiveness of the transformation we have considered many geometries of commonly used transmission lines, summarized in Fig. 2, where it is assumed that the dimensions not specified extend to infinity (i.e., they have open boundaries). They all present Transversal ElectroMagnetic (TEM) or quasi-TEM mode behavior [2], being characterized by at least two conductors. The dimensions of the geometries will be assumed to be normalized from now on since the units are not relevant in the computation of C and Z_c . Please note that, in the presented plots in this section, the label “arctan” refers to the transformation in (16), “exp”, to the transformation in (17), and “quadratic”, to the one in (18).

A. VALIDATION

The first example is the microstrip line [Fig. 2(d)], for which we have open boundaries at the top, left and right end of the domain. We selected a substrate with $\epsilon_r = 4$, $h = 0.254$ and $T = 0.0355$. Various line widths are considered in the range $w \in (0.254, 0.762)$. Our results are compared with the built-in model in LineCalc, the tool embedded in the commercial software Keysight ADS studio [27] for all presented transformations. LineCalc uses closed form approximations that have been extensively tested and it assumes an infinite size of the box. In Fig. 3(a), we can see a very good agreement in the value of Z_c between LineCalc and this work. In this example, a 10×10 box was used with its lower side centered on the line and lying on the ground plane of the microstrip, with IML of width 2 extending from the left, right, and top sides of the box.

Similar results were found for the stripline [Fig. 2(e)], shown in Fig. 3(b). The parameters were set to the same values as in the microstrip case, with a substrate of $\epsilon_r = 4$ height $h = 0.508$. Also in this case, our results were compared against the ADS model, obtaining an excellent agreement. In the case of the stripline, only the x coordinate can be transformed. Again, we considered a box of width 10, in this case with the height of the stripline, with a transformed domain of 2 on each lateral side.

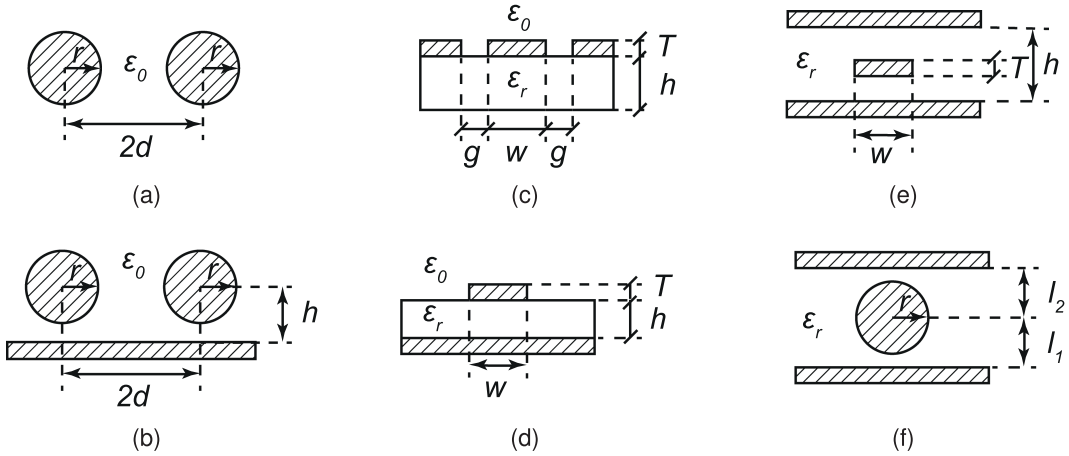


FIGURE 2. Examples of transmission lines with open boundaries characterized with the proposed technique: (a) bifilar line, (b) bifilar line with ground plane (c) coplanar line, (d) microstrip line, (e) stripline, and (f) slab line.

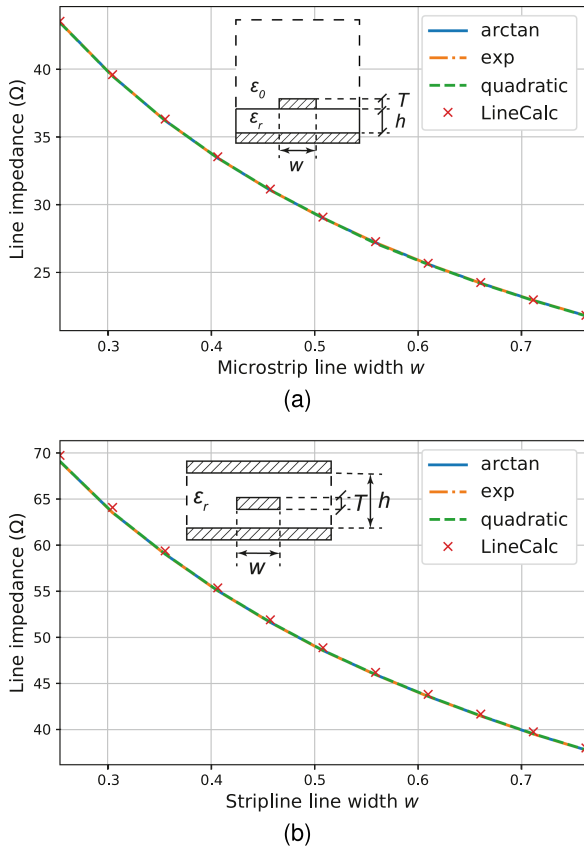


FIGURE 3. Line impedance against microstrip width, LineCalc model and our work. (a) Microstrip line with $h = 0.254$, $T = 0.0355$, $\epsilon_r = 4$. (b) stripline with $\epsilon_r = 4$, $T = 0.0355$.

B. CONVERGENCE AGAINST UNTRANSFORMED DOMAINS

To test the effectiveness of the IML for the computation of transmission line parameters, we first considered the coplanar line [Fig. 2(c)]. We have imagined this geometry enclosed in a square box and increased the size of the box towards infinity. In this case, all four directions around the line undergo the coordinate transformation.

In Fig. 4(a), we plot the value of the characteristic impedance as a function of the box size in four cases: no transformation, and with a transformation that is set in each direction to a 33% of the box side length l in all four directions [$p = 0.33$ in all sides as defined in the inset of Fig. 4(a)] for all the presented expressions (inverse tangent function, exponential function, and quadratic function). In this example, the coplanar line has a width $w = 0.508$ and a gap $g = 0.508$. The line height is set to $T = 0.035$. The dielectric has a width of $h = 0.254$ and a relative permittivity $\epsilon_r = 4$. All values for each box size have been computed with the same mesh.

Note that, in Fig. 4(a), as the box size increases all curves tend to converge towards a set value, very close to the one given by LineCalc, but applying the transformation makes the convergence much faster. In this regard, we can observe how the quadratic expression for the transformation gives the best results, followed by the inverse tangent and exponential functions.

In Fig. 4(b), the same procedure was applied to a bifilar transmission line [shown in Fig. 2(a)], which has a well-known exact expression for its impedance:

$$Z_1 = \frac{\eta_0}{\pi} \cosh^{-1} \left(\frac{d}{r} \right) \quad (24)$$

where $\eta_0 = \sqrt{\mu_0/\epsilon_0}$ is the vacuum characteristic impedance. In this case, the radius was chosen as $r = 0.254$, with a separation $d = 0.762$. Again, $p = 0.33$. In subsequent figures, the colored area defining p is omitted for the sake of clarity, since the criterion for its establishment will be identical to the one presented in Fig. 4.

The resulting curves show a very good agreement of the transformed curve with the analytical values, with the quadratic transformation function again giving the best performance. Interestingly, the inverse tangent and exponential functions give similar performances, the former being slightly better. Moreover, we can see how the untransformed problem

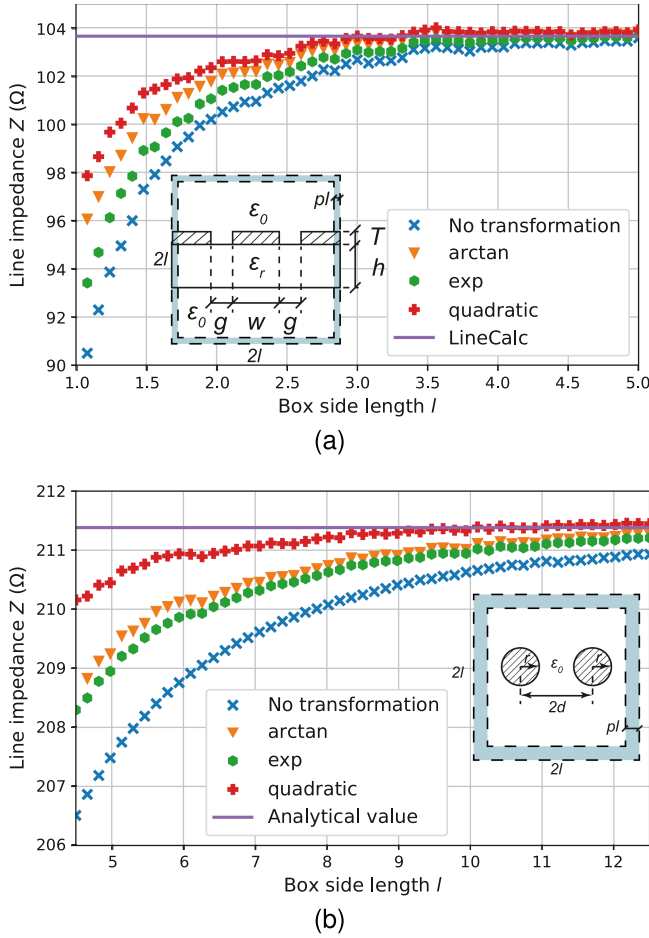


FIGURE 4. Box size and transformed area against computed line impedance. (a): coplanar line with $w = 0.508$, $g = 0.508$, $h = 0.254$, $T = 0.035$. The result given by LineCalc is displayed for reference. (b): bifilar line with $r = 0.254$, $d = 0.762$. The exact result given by (24) is also displayed for reference.

has a slow convergence, due to the fields being less confined than in the previous case, thus requiring a larger box to achieve accurate values.

C. CARTESIAN VS RADIAL TRANSFORMATION

Now, we intend to evaluate whether a radial IML might be more suitable than a Cartesian one in some cases. For that purpose, we have taken again the case of the bifilar line in Fig. 2(a) with the parameters specified in Fig. 4(b), for which its impedance has been computed in both cases using the same procedure as in Section V. In this experiment, both domains (the one with square shape as in Section secV, and the one introduced in this section with circular shape) must have similar mesh density.

In Fig. 5 it can be seen how the case with no transformation and circular domain has the worst convergence. However, applying the transformation yields very similar results for both of the transformed cases, in which the convergence is similar. For this case, only the transformation from (16) was studied. We come to the conclusion that IML can successfully

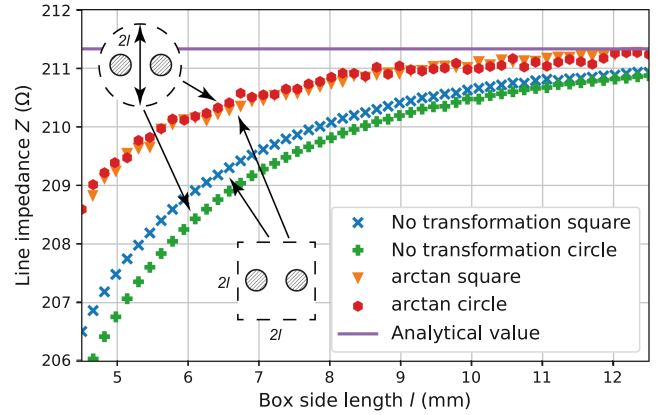


FIGURE 5. Box size and transformed area against computed line impedance using radial and Cartesian IML for the same bifilar line as described in Fig. 4(b).

be applied to a radial transformation and, even though the results are problem-dependent, it does not necessarily present a relevant advantage over its Cartesian counterpart. Furthermore, the radial transformation yields less smooth results due to the discretization of the circular IML, whereas the Cartesian transformation smoothness in the results is only subject to the relative variation of the mesh density.

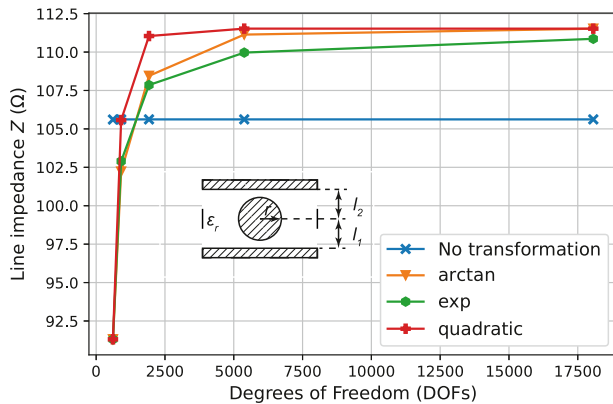
D. MESH CONVERGENCE OF THE TRANSFORMATION

To check the effect of the mesh density on the transformation, we take the slab line in Fig. 2(f). It has a radius of $r = 2.54$, which is placed in the middle of two metallic planes separated $l_1 + l_2 = 2l_1 = 10.16$ between them. In this experiment we take a box of width 6, taking a transformation of size 2 on each side. The problem was simulated for different number of Degrees of Freedom (DOF) inside the IML, while keeping the dimensions and the mesh inside the untransformed domain the same in all cases. Both the domains with and without IML have the exact same box size. Examples of the meshes are shown in fig. 6(b), 6(c).

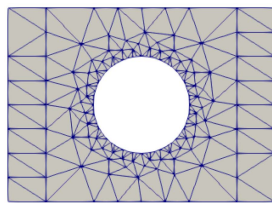
In Fig. 6(a), it can be observed that the results for the untransformed case (blue line) barely change when increasing the mesh density on the IML area (in this case without applying an IML). On the other hand, for the transformed case, a finer mesh in the IML area is needed to obtain convergent results (which are expected to be closer to the actual impedance of the structure in comparison to the untransformed case). This difference in mesh convergence is due to the artificial material $\bar{\epsilon}_r'$ from (14), which needs a certain amount of DOFs to be accurately discretized. As for the transformations, it is interesting to note that, again, the quadratic transformation has the better convergence rate on a coarse mesh, while the exponential function is the worst performer, even on a very fine mesh.

E. LIMITS OF THE TRANSFORMATION PROCEDURE

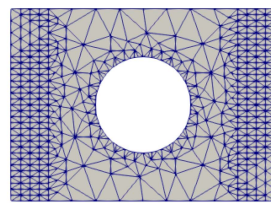
The starting point of the transformation (x_1, y_1) is a key parameter that must be chosen reasonably, since, as an effect of



(a)



(b)



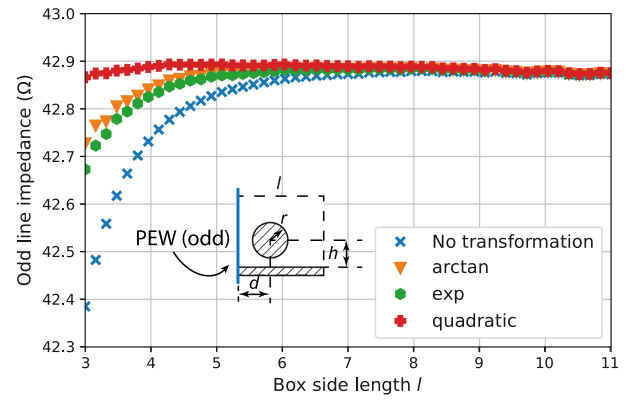
(c)

FIGURE 6. (a) Computed line impedance against number of total DOFs for the untransformed and transformed case. The fixed box size does not lead to an accurate characteristic impedance for the untransformed case. The number of DOFs is increased only in the IML subdomain, both for the transformed and untransformed case. (b) Mesh corresponding to the leftmost values in Fig. 6(a). (c) Mesh corresponding to the second to the leftmost values in Fig. 6(a).

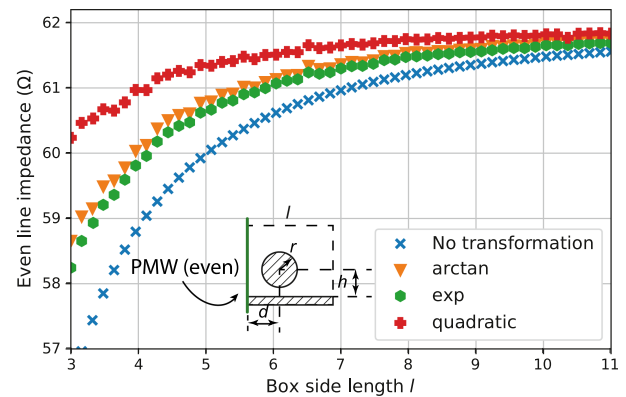
FEM discretization, there is a limit on how close to the finite metals and dielectrics this procedure can be applied to. At the same time, the thickness of the transformed region should not be too small.

To analyze this combined effect, we have chosen the case of the geometry in Fig. 2(b), and we consider the problem with an even or odd symmetry (i.e., boundary conditions associated to a perfect electric or magnetic conductor) along the center line. The dimensions for the line are $r = 0.254$, $d = 0.762$ and $h = 0.762$.

Fig. 7 shows the usual convergence plot in which the box size is gradually increased and the IML are set as a percentage of the box side length l , namely 33%. Starting from a minimum box size, we compare the results obtained by transforming the region beyond the minimum size to those obtained by not transforming it. When the box size is minimum (3.0) the results with and without transformation are non-convergent. By increasing the size of the box, the convergence of the transformed geometry is much faster than that of the untransformed one. Note that, in Fig. 7, the impedance for the odd mode varies a 0.4% throughout the graph, while the impedance for the even mode varies approximately 4%. This is due to the field distribution, which depends on the geometry of the problem, and is one of the reasons why IML should be considered when looking for reliable, convergent results in electrostatic problems.



(a)



(b)

FIGURE 7. Box size and transformed area against computed line impedance for a grounded bifilar line with (a) odd and (b) even symmetries in the center axis. Dimensions: $r = 0.254$, $d = 0.762$ and $h = 0.762$ [see Fig. 2(d)].

Fig 8 shows results obtained by a different type of analysis: the box size is kept fixed to $l = 4.5$ and the size of the transformed region is changed gradually from $p = 0$ to $p = 3.5$. The odd mode impedance is shown in Fig. 7(a) (the most accurate value is around 42.85Ω), while the even mode impedance is shown on Fig. 7(b) (the most accurate value is around 61.90Ω). When the transformation area is very thin, all transformations yield similar results. They have different convergence rates, as can be seen in the middle part of the graphs, but should yield the exact same convergent results. For the both the even and odd line impedances in Fig. 8 we cannot identify a limit on the transformation procedure (values do not become incoherent on the right side of the plot). However, for the even line impedance, convergence is not reached in this experiment, which means that a larger box size is needed (as it was shown in Fig. 7).

As a rule of thumb, one should ensure that a few FEM elements (not just one) are present in the transformed region and a few FEM elements (not just one) are present between the conductors and the transformed region. Although this is a rather coarse rule, its application is very easy to check and to implement.

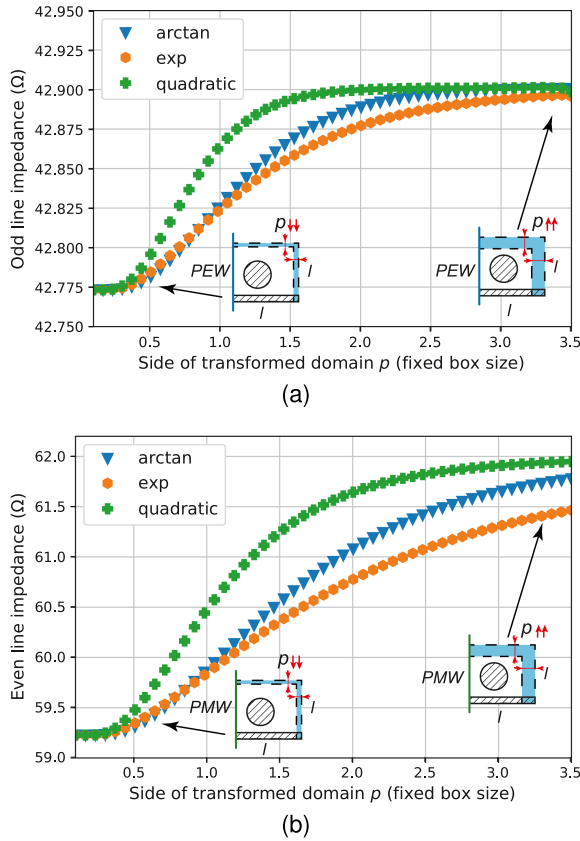


FIGURE 8. Side of transformed domain against computed line impedance for a fixed box size ($l = 4.5$) for the grounded bifilar line described in Fig. 7. (a) Odd line impedance and (b) even line impedance. The value of p is increased without modifying l , which can yield non-convergent results, as is the case in (b).

F. VISUALIZING THE TRANSFORMATION

To visualize the transformation in terms of potentials Φ and Φ' and vector fields \mathbf{E} and $\mathbf{E}' = (\mathbf{J}^T)^{-1}\mathbf{E}$ with the Jacobian \mathbf{J} given by (14), we have taken the slab line case, displayed in Fig. 2(f). In this case, the transformation is performed only on the x direction (the infinite boundaries are in $x \rightarrow \pm\infty$), which simplifies the visualization of the potential functions. In Fig. 9, we have taken a slab line of radius $r = 2.54$, which is placed in the middle of two metallic planes separated $l_1 + l_2 = 2l_1 = 10.16$ between them. Fig. 9(a) shows the potential Φ and field pattern \mathbf{E} in the untransformed domain, while for Fig. 9(b) Φ' and \mathbf{E}' are displayed, with 3 transformed on each side using the technique described in this work (using the quadratic transformation), whose subdomains can be easily identified in the figure, as they have straight vertical boundaries with the untransformed part of the domain.

It can be seen how, close to the limits towards $\pm x$, the electric field for the untransformed case still has a noticeable magnitude even though it should be close to null (the procedure yields an impedance of approximately 108Ω). However, for the transformed case, we can observe a rapid decay of the potential function once the IML starts, having, as desired, a close to null electric field towards the end of the domain in

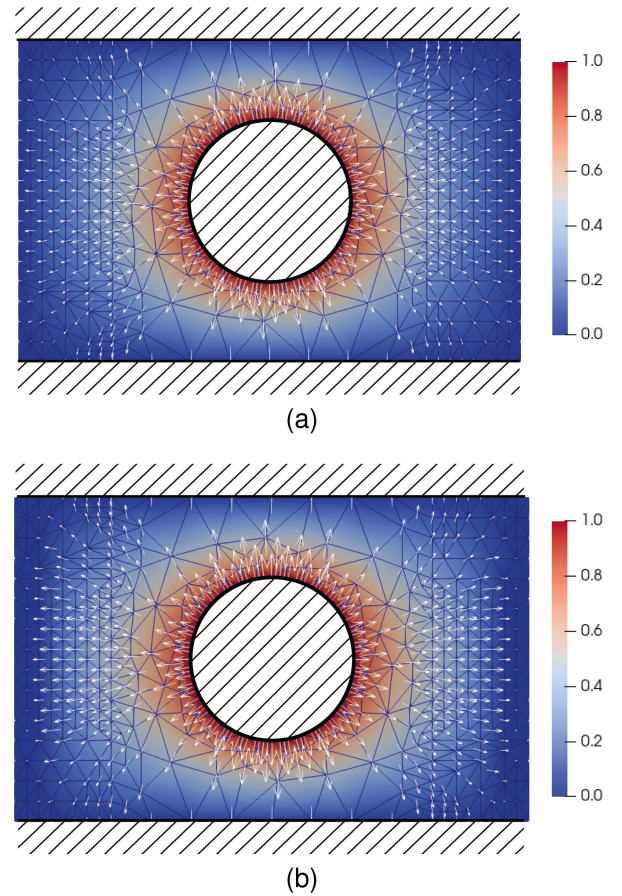


FIGURE 9. Visualizing the effect of the transformation in the problem of the slab line in Fig. 2(f) ($l_1 + l_2 = 2l_1 = 10.16$, $r = 2.54$): (a) Φ and \mathbf{E} field (white arrows) in the original domain. (b) Φ' and \mathbf{E}' field (white arrows) in the transformed domain. In the real problem, the box dimension in the horizontal axis extends to infinity.

$\pm x$ (the obtained impedance is now 111Ω). This is representative to how the IML is “compacting” the space through the geometrical transformation.

VI. CONCLUSION

The use of geometrical transformations and Infinite Mapping Layers to model open boundaries in the two-dimensional Finite Element Method for transmission line problems is presented for both Cartesian and radial transformations. It is based on solving an equivalent finite domain problem where the material has the transformation mapping taken into account. The application is demonstrated by fully characterizing (in line parameters and fields) the TEM and quasi-TEM modes for several open transmission lines. The advantages in terms of reliability of the results are very significant, thanks to the compactness of the domain of analysis, as it has been shown with several examples commonly used in the microwave arena. The approach does not need any changes in either the FEM formulation or the mesh, which can be unstructured. Moreover, it has been found that the proposed quadratic-like transformation is the most suitable for this problem, and that

a certain mesh density is required to obtain accurate results when implementing Infinite Mapping Layers.

APPENDIX PROOF OF (15)

Let's consider a 2-D transformation $\mathbf{r} \rightarrow \mathbf{r}'(\mathbf{r})$ that admits a unique inverse $\mathbf{r} = \mathbf{r}'(\mathbf{r}')$. For an arbitrary function $\psi(\mathbf{r})$ we have that

$$\int_{\Omega} \psi(\mathbf{r}) dx dy = \int_{\Omega'} \psi[\mathbf{r}'(\mathbf{r}')] \det \left(\frac{\partial \mathbf{r}}{\partial \mathbf{r}'} \right) dx' dy' \quad (25)$$

and

$$\det \left(\frac{\partial \mathbf{r}}{\partial \mathbf{r}'} \right) = \left[\det \left(\frac{\partial \mathbf{r}'}{\partial \mathbf{r}} \right) \right]^{-1} = (\det \mathbf{J})^{-1}. \quad (26)$$

Letting then $\psi(\mathbf{r}) = \Phi(\mathbf{r}) = \Phi'[\mathbf{r}'(\mathbf{r})]$ and being $\nabla \Phi = \mathbf{J}^T \nabla' \Phi'$, we have $\nabla \Phi \cdot \bar{\epsilon}_r \nabla \Phi = \nabla' \Phi' \mathbf{J} \cdot \bar{\epsilon}_r \mathbf{J}^T \nabla' \Phi'$. Thus, we conclude that (15) follows.

REFERENCES

- [1] J.-S. Chang, A. J. Kelly, and J. M. Crowley, *Handbook of Electrostatic Processes*. Boca Raton, FL, USA: CRC Press, 1995.
- [2] R. E. Collin, *Field Theory of Guided Waves*. Piscataway, NJ, USA: Wiley, 1990.
- [3] D. Y. Heh and E. L. Tan, "Multiple LOD-FDTD method for multi-conductor coupled transmission lines," *IEEE J. Multiscale Multiphys. Comput. Techn.*, vol. 5, pp. 201–208, 2020.
- [4] S. S. Sawant, Z. Yao, R. Jambunathan, and A. Nonaka, "Characterization of transmission lines in microelectronic circuits using the ARTEMIS solver," *IEEE J. Multiscale Multiphys. Comput. Techn.*, vol. 8, pp. 31–39, 2023.
- [5] Y. Yi, Z. Chen, W. Tang, and L. Wang, "Calculation of ion flow environment of DC transmission lines in the presence of charged aerosol particulates based on upwind-FEM," *Electric Power Syst. Res.*, vol. 184, 2020, Art. no. 106289.
- [6] A. Milovna novic Dr and B. Koprivica, "Approximate calculation of characteristic parameters of rectangular transmission lines," *Inf. Technol. Elect. Eng. – Devices Syst., Mater. Technol. Future*, vol. 54, 2009.
- [7] S. T. Todd, X. T. Huang, J. E. Bowers, and N. C. MacDonald, "Fabrication, modeling, and characterization of high-aspect-ratio coplanar waveguide," *IEEE Trans. Microw. Theory Techn.*, vol. 58, no. 12, pp. 3790–3800, Dec. 2010.
- [8] E. Costamagna, "On the numerical inversion of the schwarz-christoffel conformal transformation," *IEEE Trans. Microw. Theory Techn.*, vol. 35, no. 1, pp. 35–40, Jan. 1987.
- [9] G. Pelosi, R. Coccioli, and S. Selleri, *Quick Finite Elements Electromagn. Waves* (Artech House Electromagn Series). Norwood, MA, USA: Artech House, 2009.
- [10] J. Jin, *The Finite Element Method in Electromagnetics*, Hoboken, NJ, USA: Wiley, 2015.
- [11] P. Brown, "A non-interactive method for the automatic generation of finite element meshes using the Schwarz-Christoffel transformation," *Comput. Methods Appl. Mech. Eng.*, vol. 25, no. 1, pp. 101–126, 1981.
- [12] E. Melgoza and R. Escarda, "Mapped infinite elements for the solution of open electric and magnetic field problems," in *Proc. IEEE Int. Autumn Meeting Power, Electron. Comput.*, 2014, pp. 1–6.
- [13] Y. Zhu and A. C. Cangellaris, *Multigrid Finite Element Methods for Electromagnetic Field Modeling*, vol. 28. Hoboken, NJ, USA: Wiley, 2006.
- [14] D. C. Meeker, "Improvised asymptotic boundary conditions for electrostatic finite elements," *IEEE Trans. Magn.*, vol. 50, no. 6, Jun. 2014, Art. no. 7400609.
- [15] G. Aiello, S. Alfonzetti, E. Diletto, and N. Salerno, "An iterative solution to FEM-BEM algebraic systems for open-boundary electrostatic problems," *IEEE Trans. Magn.*, vol. 43, no. 4, pp. 1249–1252, Apr. 2007.
- [16] B. Stupfel and R. Mittra, "A theoretical study of numerical absorbing boundary conditions," *IEEE Trans. Antennas Propag.*, vol. 43, no. 5, pp. 478–487, May 1995.
- [17] J.-P. Berenger, "A perfectly matched layer for the absorption of electromagnetic waves," *J. Comput. Phys.*, vol. 114, no. 2, pp. 185–200, 1994.
- [18] F. Toth, S. Schoder, and M. Kaltenbacher, "An infinite mapping layer for deep water waves," in *Proc. Appl. Math. Mech.*, vol. 17, no. 1, pp. 689–690, 2017.
- [19] S. Schoder, F. Toth, C. Freidhager, and M. Kaltenbacher, "Revisiting infinite mapping layer for open domain problems," *J. Comput. Phys.*, vol. 392, pp. 354–367, 2019.
- [20] D. Shyrok, "Squeezing of open boundaries by Maxwell-consistent real coordinate transformation," *IEEE Microw. Wireless Compon. Lett.*, vol. 16, no. 11, pp. 576–578, Nov. 2006.
- [21] U. Leonhardt, "Optical conformal mapping," *Science*, vol. 312, pp. 5781, pp. 1777–1780, 2006.
- [22] J. B. Pendry, D. Schurig, and D. R. Smith, "Controlling electromagnetic fields," *Science*, vol. 312, no. 5781, pp. 1780–1782, 2006.
- [23] H. Chen, C. T. Chan, and P. Sheng, "Transformation optics and metamaterials," *Nature Mater.*, vol. 9, no. 5, pp. 387–396, 2010.
- [24] G. Plaza, F. Mesa, and M. Horno, "Quick computation of (C), (L), (G), and (R) matrices of multiconductor and multilayered transmission systems," *IEEE Trans. Microw. Theory Techn.*, vol. 43, no. 7, pp. 1623–1626, Jul. 1995.
- [25] G. Gentili and M. Salazar-Palma, "The definition and computation of modal characteristic impedance in quasi-TEM coupled transmission lines," *IEEE Trans. Microw. Theory Techn.*, vol. 43, no. 2, pp. 338–343, Feb. 1995.
- [26] A. Morán-López, J. Córcoles, and J. A. Ruiz-Cruz, "Efficient computation and orthonormalization of multiple TEM numerical modes arising from fem for microwave computer-aided-design," in *Proc. IEEE MTT-S Int. Conf. Numer. Electromagn. Multiphys. Model. Optim. RF, Microw., THz Appl.*, 2017, pp. 197–199.
- [27] Keysight, "Pathwave advanced design system (ADS)," 2020. Accessed: Apr. 14, 2024. [www.keysight.com. https://www.keysight.com/us/en/products/software/pathwave-design-software/pathwave-advanced-design-system.html](https://www.keysight.com/us/en/products/software/pathwave-design-software/pathwave-advanced-design-system.html)



GINES GARCIA-CONTRERAS was born in Madrid, Spain, in 1997. He received the B.Sc. and M.Sc. degrees in electrical engineering from Universidad Autónoma de Madrid, Madrid, Spain, in 2019 and 2021, respectively. Since 2021, he has been currently working toward the Ph.D. degree in applied electromagnetics with the "Radiofrecuencia: Circuitos, Antenas y Sistemas" Research Group, UAM. From April 2022 to June 2022, he was a Visiting Scholar with the Politecnico di Milano, Milan, Italy, and with KTH Royal Institute of Technology, Stockholm, Sweden, from October 2023 to December 2023. His research interests include numerical and hybrid methods for the design of microwave passive components, symmetries, and periodic structures.



JUAN CÓRCOLES (Senior Member, IEEE) was born in Albacete, Spain, in 1981. He received the Ingeniero de Telecomunicación degree (B.Sc. and M.Sc. degrees in electrical engineering) and the Ph.D. degree from the Universidad Politécnica de Madrid, Madrid, Spain, in 2004 and 2009, respectively. From 2010 to 2023, he was with the Universidad Autónoma de Madrid, Madrid, Spain, where he became an Associate Professor in 2015. Since 2023, he has been with Universidad Politécnica de Madrid. His research interests include applied and computational electromagnetics, particularly in the development of numerical methods and optimization techniques for the analysis and design of microwave circuits, antennas, and other related applications.



JORGE A. RUIZ-CRUZ received the Ingeniero de Telecomunicación and Ph.D. degrees from the Universidad Politécnica de Madrid (UPM), Madrid, Spain, in 1999 and 2005, respectively. Before starting the Ph.D. program, he was with the company RYMSA in 2000. After finishing the Ph.D., he was a Research Associate with the University of Maryland, College Park, MD, USA. In 2006, he joined Universidad Autónoma de Madrid, where he became Associate Professor in 2009 and Full Professor in 2021. In 2023 he joined the UPM,

as a Full Professor with the Department of Signals, Systems and Radio-communications. His research interests include the computer-aided design of microwave passive devices and systems (filters, multiplexers, and orthomodes).



GIAN GUIDO GENTILI received the Laurea degree in electronics engineering from the Politecnico di Milano, Milan, Italy, in 1987. In 1989, he became a Researcher with the Dipartimento di Elettronica ed Informazione, National Research Council, Center for Space Telecommunications, Politecnico di Milano. In 2001, he became a Senior CNR Researcher. In 2002, he became an Associate Professor with the Politecnico di Milano. He was Visiting Scholar with Politecnica de Madrid, Madrid, Spain, in 1993 and 1995, respectively. He

is responsible for the Electromagnetics Laboratory of Politecnico di Milano “Wavelab.” His research interests include numerical method for electromagnetics (finite elements, method of moments, and mode-matching), antennas and feed systems for terrestrial and space applications, microwave passive devices and filters, plasmonics, and terahertz radiation.



MATTEO OLDONI (Member, IEEE) was born in 1984. He received the Ph.D. degree in information technology from Politecnico di Milano, Milan, Italy, in 2013. He was a Microwave Designer in Research and Development of microwave components for a private multinational company until 2022, when he joined the Electronics and Information department of Politecnico di Milano as a Researcher. His research interests include synthesis and design techniques for microwave filters, algorithms development for computer-aided tuning, and antenna design.

ing, and antenna design.



LORENZO CODECASA (Member, IEEE) received the Ph.D. degree in electronic engineering from the Politecnico di Milano, Milan, Italy, in 2001. From 2002 to 2010, he been an Assistant Professor of electrical engineering with the Department of Electronics, Information, and Bioengineering, Politecnico di Milano. Since 2010, he has been an Associate Professor of electrical engineering with the same Department. He has authored or coauthored over 220 papers in refereed international journals and conference proceedings in his main

research areas, which include the theoretical analysis and in the computational investigation of electric circuits and of electromagnetic fields, with particular emphasis on thermal management of electronic components. In these activities, he has introduced original industrial-strength approaches, some of which are currently implemented in market leader simulation software. For his researches, he was the recipient of three conference Best Paper Awards and Harvey Rosten Award for Excellence. He is an Associate Editor for IEEE TRANSACTIONS OF COMPONENTS, PACKAGING AND MANUFACTURING TECHNOLOGY and was the Program Chair of the conference THERMAL Investigation of Integrated Circuits (THERMINIC).